Performance Improvement of Concentrated Solar Thermal Collectors using Ti and AlN Composite Coatings for Photothermal Conversion Applications

Mutawalli Bello*, Abdulrasheed Nuhu
Department of Physics, Federal College of Education,
P.M.B 2042 Yola, Adamawa, Nigeria
*E-mail address: mutawallibello2018@gmail.com
DOI: 10.56201/ijemt.vol.11.no4.2025.pg11.22

Abstract
Despite numerous attempts and achievements recorded so far towards photothermal conversion of radiant energy from the sun for power generation, the attention on improving the existing systems towards achieving high efficiency has given less attention. In this perspective, we have synthesized Ti and AlN thin film multilayer solar absorber coatings used in improving concentrated solar collectors for power generation. The coatings was deposited onto a modified stainless steel substrate using Direct Current (DC)/Radio Frequency (RF) magnetron sputtering at room temperature. The coating exhibited high solar absorptance of 0.91 and low thermal emittance of 0.15 in the solar and infrared regions respectively. The coatings was found to be structurally, optically and thermally stable up to a temperature of about 450 ^{o}C in ambient air. The adhesion test analysis revealed that the coated layers are well adhered to one another and on to the substrate. These results indicate the present coatings has the potentials in improving high temperature concentrated collectors for photothermal conversion application.

Keywords: *Photothermal conversion, Radiant energy, Thin film, Imagin camera,*

1. Introduction

It became imperative to explore other alternative source of energy due to increasing demand for electricity. Solar energy is a good candidate alternative as it is a clean, green and environmentally friendly which can be herness using simple technology such as concentrating solar power (CSP) system to meet up with the increasing demand for the energy. The efficiency of these systems can be enhanced through application of spectrally selective absorber coatings that is capable of absorbing solar radiation within the wavelength range of 300 nm to 2500 nm and emit less at the infrared region beyond a wavelength of 5000 nm. Achieving these desired characteristics is practically impossible using single materials [1], [2].

Multilayer selective solar absorber coatings can be designed using layers of different as interference stack [3]. Therefore, materials such as metal Ti and dielectric AlN will be suitable for this purpose due to its outstanding properties such as high melting point and resistant to corrosion among others. A lot of research using metals like Mo, Ni, Ag and Cu alongside dielectrics such as Al_2O_3, ZnO, CuO_2 and SiO_2 has been carried out as solar absorber coatings for high temperature application [3]. The table 1 summarizes some of the recent literatures in developing SSACs.

Table 1 Summary of different configurations, optical properties, and thermal stability of some high temperature physical vapour deposited solar selective absorber coatings.

Materials	Deposition method	Subs.	Thickness (nm)	*α* (%)	*ε* (%)	Therm. Stab. ºC		Ref.
						Vac.	Air	
TiB_2/Ti(B,N)/SiON/SiO_2	Sputtering	SS	255	0.784	0.15	400	-	[4]
Ti/TiB_2/Ti(B,N)/SiON/SiO_2	Sputtering	SS	255	0.981	0.15	450	-	[4]
$Ti_{1-x}Al_xN$	Sputtering	SS	284	0.92	0.04	900	-	[5]
$TiN_x/TiN_{x1}O_{y1}/TiN_{x2}O_{y2}$	Sputtering	SS	308	0.946	0.38	-	250	[6]
$Cr_{1-x}Al_xN_y$	Sputtering	SS	550	0.95	0.15		500	[7]
W/WAlN/WAlON/Al_2O_3	Sputtering	SS	205	0.96	0.08	-	350	[8]
AlCrMoTaTiN/Al_2O_3	Sputtering	SS	122	0.929	0.082	500	300	[9]
NbMoTaWN	Sputtering	SS	240	0.936	0.126	500	400	[10]
TiAlC/TiAlCN/TiAlSiCN/TiAlSiCO/TiAlSiO	Sputtering	SS	943	0.960	0.15	500	-	[11]

Ti/AlN/Ti	Sputtering	SS	85	0.89	0.19	-	500	[2]
SS-(Fe3O4)/Ti/AlN/Ti/SiO2	Sputtering	SS	85	0.96	0.2	-	500	[12]

Despite good performance exhibited by these coatings in terms of high solar absorptance and low thermal emittance, the material combinations is too cumbersome as it involves several layers which in turn leads to the high thickness of overall coating. Moreover, high thickness is not recommended for large scale industrial production as it consume a lot of materials which will in turn increase the overall cost.

In this contribution, we developed an ultra-thin (~55 nm) thickness solar absorber coating using made DC/RF magnetron co-sputtering of Ti and AlN at room temperature on to modified stainless steel substrate. After which, the structural, compositional, morphology, topology, spectral selectivity and the adhesion test were carried out. The result revealed that the present coating exhibited good solar absorptance with low thermal emittance. The scratch adhesion test shows that the coated layers demonstrated good adhesion between them and to the substrate.

2. Experimental Details

2.1 Sample preparation

The silicon substrate was cleaned in accordance with the well-known standard procedure of the Radio Corporation America (RCA). In this method, three different solutions such as $H_2O/NH_4OH/H_2O_2$, HF/H_2O and $H_2O/HCL/H_2O_2$ with volume ratio (mL) 5:1:1, 1:5 and 6:1:1 respectively were prepared. The Si substrate was cleaned in the three solutions at a temperature between 75 ^oC to 80 ^oC for 10 minutes, 20 seconds and 10 minutes respectively and rinsed with DI water and then finally dried with nitrogen purge to remove any possible oxide layer on the wafer. The final step in the cleaning process usually create a thin passivating layer on the surface of the Si wafer which prevents it from further contaminations.

The cleaned substrates were fixed on the substrate's holder which was kept rotating continuously during the deposition to ensure uniform coating. High purity metallic Ti (purity 99.99%) and dielectric AlN (purity 99.99%) targets were used under Ar plasma to deposit Ti and AlN coating. The targets were fixed onto the magnetron and the chamber was closed. The metal Ti target was powered by DC source and the dielectric AlN were powered from the RF power source. A vacuum chamber pressure of 5.0×10^{-5} mbar was attained by pumping down the chamber using turbo mechanical pump. The sputtering power was ON, and the targets were cleaned *in situ* plasma cleaning for 15 minutes by Ar ion bombardments to remove impurities that might have been embedded on it. Later the shutter was opened, and the deposition was carried out at room temperature. The thickness and the deposition rates were recorded from the digital crystal (thickness) monitor installed in the machine.

2.2 Characterization

The Structural properties were investigated with the aid of High-resolution X-Ray diffractometer (HR-XRD) (Model: PANalytical X'pert PRO MRD PW3040). The chemical composition was studied using Energy-dispersive X-ray Spectroscopy (EDX). Morphology of the prepared film was studied using, Field Emission Scanning Electron Microscope (FESEM) (Model: FEI Nova NanoSEM 450). The grain size of the prepared sample was calculated using Image J software. The topology and surface roughness were investigated using Atomic Force Microscopy (AFM) (Model: Dimension EDGE, BRUKER). Optical properties of the coatings over 300-2500 nm wavelength range were measured using Carry 500 UV-Vis-NIR spectrophotometer.

The adhesion test was investigated using Taber Shear/Scratch Tester (model: 551). The test was performed under constant load condition during the indenter stroke in accordance with the ASTM C 1624-05 and the mean scratch width was measured using a powerful microscope.

3. Results and discussion

3.1 Structural properties

Fig. 1 depicts the XRD patterns of TiAlN composite thin film coating deposited onto Fe_3O_4 modified SS substrate. The sharp diffraction peak with the highest intensity located at 2θ=74.76° correspond to the reflection from the used SS substrate. Four (4) other diffraction peaks were identified and located at 2θ=27.10°, 35.46°, 43.82° and 50.45° correspond to the planes of (214), (422), (434) and (346) highly crystalline Fe_3O_4 from the modified SS substrate. This result is in good agreement with our earlier works on multilayer coatings reported elsewhere [2], [12]. Similarly, planes of (101) and (110) phases of crystalline AlN were identified and are located at an angular position of 2θ=37.90° and 59.32° respectively. These peaks are similar to the crystallographic peaks reported in the literature elsewhere [13]. Furthermore, one weak and broad diffraction peaks located at 2θ=64.91° and 82.18° are related to phases of Ti (220) and (222) respectively. The increaser in the intensity of (222) compared to the ones we reported earlier in the literature [12], [14] was noticed. The increase in the intensity of (222) oriented peak could be associated with the co-sputtering of the Ti and AlN in which the AlN serve as a buffer to the Ti. To further confirm the presence of Ti and AlN, and the Fe_3O_4, an EDX analysis alongside its corresponding electron image (inset) depicted in Fig. 2 confirmed its presence. The crystallite size (D) was calculated using Debye Scherrer's equation given by Eq. 1.

$$D = \frac{K\lambda}{\beta cos\theta} \qquad (1)$$

Where *D, K, λ, β* and *θ* are the average crystallite size in (nm), grain shape factor (0.94), wavelength of the incident X-ray, full width half maximum (FWHM) in radians and Bragg's diffraction angle respectively. The average grain size was about 45.80 nm.

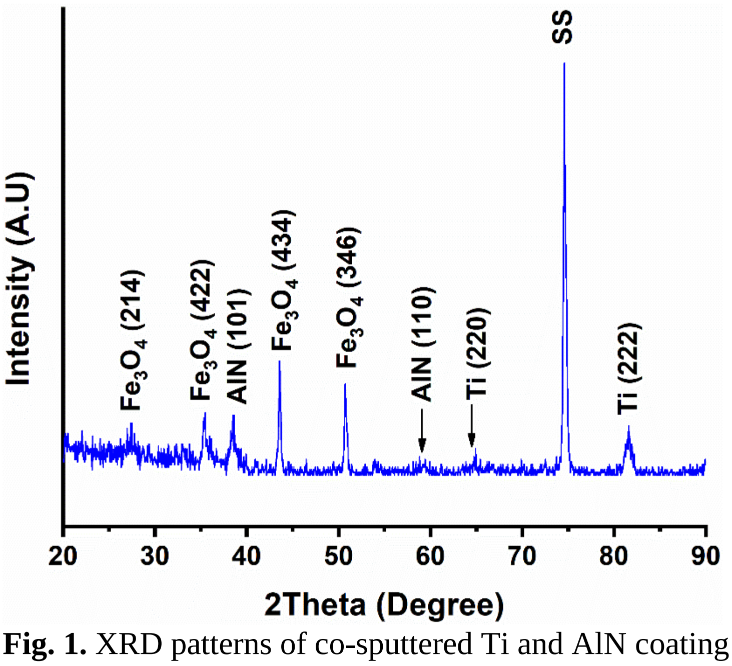

Fig. 1. XRD patterns of co-sputtered Ti and AlN coating on Fe_3O_4 modified SS substrate

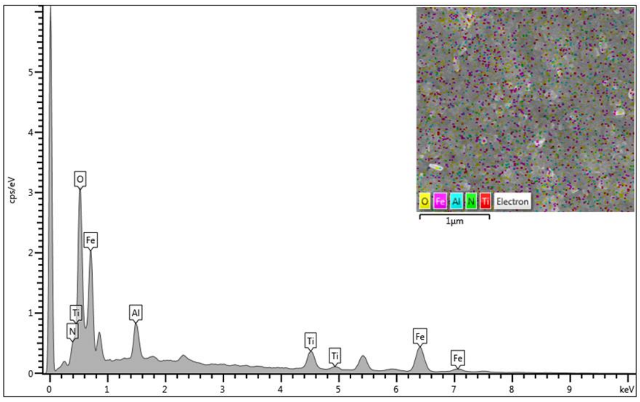

Fig. 2. EDX spectrum of co-sputtered Ti and AlN coating on Fe_3O_4 modified SS substrate

3.2 Surface and cross-sectional morphologies

Fig. 3 (a-d) shows the FESEM images of co-sputtered Ti and AlN thin film coating deposited onto the Fe_3O_4 modified SS substrate and its corresponding thicknesses as shown in Fig. 3 (e-h). The thickness of the first layer was optimized as 25 nm. After which, four other samples were refabricated with the optimum (25 nm) bottom layer and annealed. The second layer of various thicknesses ranging from 10 nm- 40 nm was deposited on each of the samples. The surface of the sample with approximately 10 nm thickness of co-sputtered Ti and AlN second layer (Fig. 3a) is stacked with continuous dense "sponge-like" nano structures with average diameter of 32.40 nm. The size of the nano structures was observed to be increasing with the increase in the film thickness to 20 nm, 30 nm and 40 nm as evident from Fig. 3b-d with average diameter of 37.92 nm, 42.17 nm and 53.24 nm respectively. However, at 40 nm thickness (Fig. 3d), an agglomeration of nanoparticles forming a larger "worm-like" structures were observed. The approximate corresponding of thickness of each sample is depicted in the cross-sectional images shown in Fig. 3(e-h). The small discrepancies in targeted thickness and the measured thickness could be associated with the errors while drawing the lines.

Fig. 4 (a-d) shows the 3D AFM images of co-sputtered Ti and AlN composite thin film deposited onto modified SS substrate at different thickness. The surface of the sample with 10 nm thickness of second layer (Fig. 4a) exhibits small textured growth in the vertical direction of the substrate as expected for a sputtered coating grown at room temperature [12], with average roughness of 53.4 nm. A significance improvement in the growth was noticed when the film thickness of the second layer was increased to 20 nm resulting to further increase in the average surface roughness to 61.7 nm as shown in Fig. 4b. The textured surface become more pronounced with the thickness of the second layer was increased to 30 nm and 40 nm as evident from Fig. 3c and 3d with a corresponding increase in the average roughness of 73.2 nm and 85.1 nm respectively. The surface roughness plays a vital role in the solar absorption as the incidence light striking its surface suffers multiple and are been trapped within the surface thereby increasing the overall efficiency. Moreover, surface roughness between 10 nm to 100 nm range support multiple reflection and subsequently trapping the reflected incident light and hence, enhances solar absorption [15]. Comparatively, this surface roughness is correlated to the particle size (diameter of the nano particles) as obtained from the FESEM analysis.

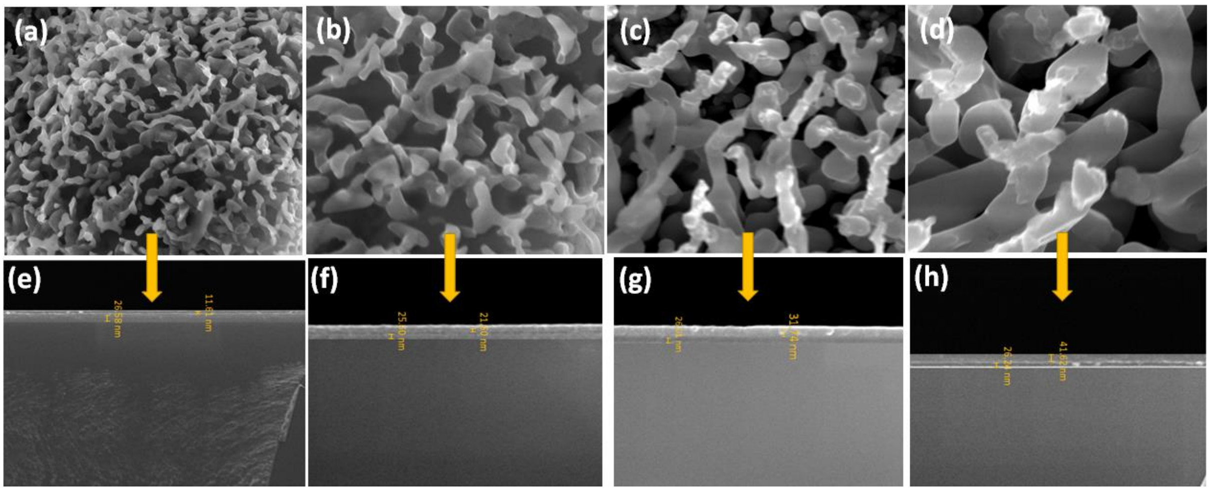

Fig. 3. FESEM images and its corresponding cross-section of co-sputtered Ti and AlN coating on Fe_3O_4 modified SS substrate

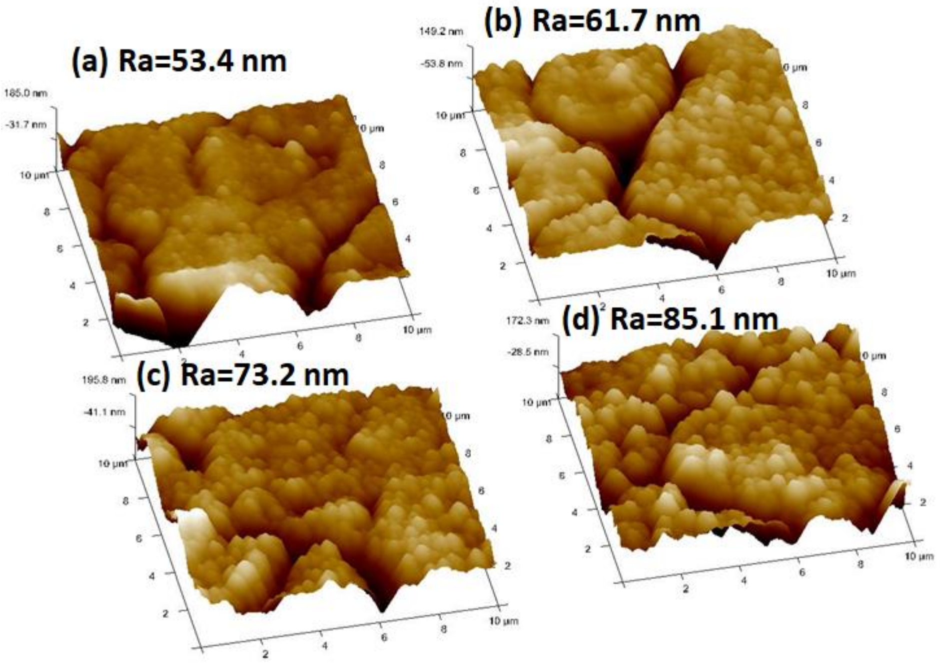

Fig. 4. 3D AFM images of co-sputtered Ti and AlN coating on Fe_3O_4 modified SS substrate

3.3 Reflectance spectra

Fig. 5 shows the reflectance spectra of co-puttered Ti and AlN composite coating at various thicknesses deposited onto modified SS substrate. The reflectance from the pristine and annealed substrate is used as a reference. From the Fig., it can be observed that the pristine SS substrate exhibits high reflectance, and it is increasing with the increase in the wavelength, thus indicating that SS substrate is a good candidate for photothermal conversion application. The reflectance from the pristine substrate was suppressed after modification of the substrate by simple annealing. This reduction in the reflectance was due to the absorption of solar radiation by the Fe_3O_4 that was formed as a result of the modification of the substrate. The reflectance was further supressed significantly after deposition of the Ti and AlN composite second layer of thicknesses 10 nm, 20 nm and 30 nm, and thus, indicating good solar absorptance. However, when the thickness was increased to 40 nm, a sharp increase in the reflectance spectra was noticed especially between the wavelength range of 800 nm and above, thereby reduces the solar absorptance. Generally, thicker coatings lead to low solar absorptance, high infrared emittance and peel-off. The sharp peaks between the wavelength range of 300 nm to 400 nm is due to the interaction between the incident and reflected light.

The solar absorptance was calculated from the measured reflectance data $R(\lambda)$ using equations 2 and weighted average by spectral solar irradiance $I(\lambda)$ using AM 1.5 as defined by ISO standard 8945-1 (1992) [16]. The result obtained is depicted in Fig. 6.

$$\alpha = \frac{\int_{\lambda_1}^{\lambda_2} (1 - R(\lambda)) I(\lambda) d(\lambda)}{\int_{\lambda_1}^{\lambda_2} I(\lambda)\, d(\lambda)} \tag{2}$$

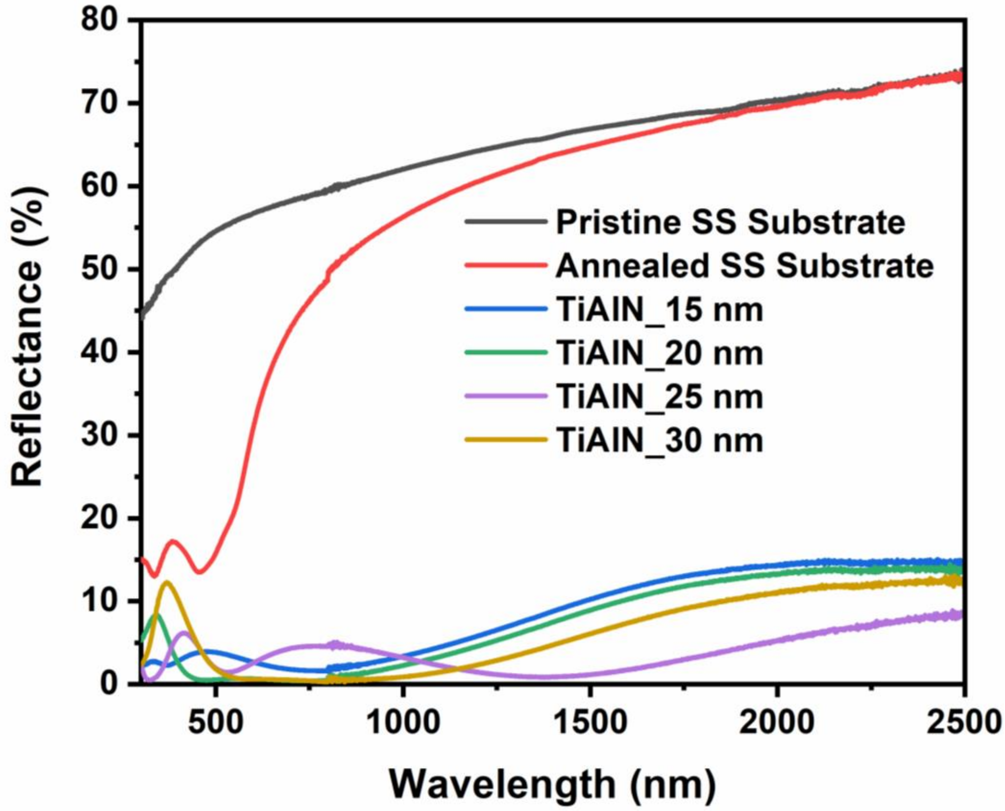

Fig. 5. Reflectance spectra of co-sputtered Ti and AlN composite coating deposited onto modified SS substrate.

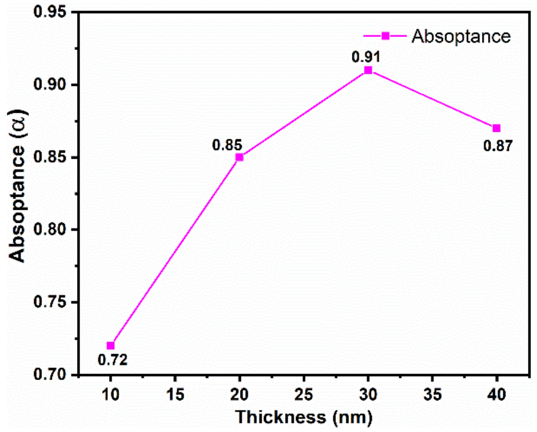

Fig. 6. Solar absorptance of co-sputtered Ti and AlN composite coating deposited onto modified SS substrate.

3.4 Adhesion test result

The adhesion strength of any solar absorber coating determines its functionality especially at elevated temperatures. The adhesion failure between the coated layers (in the case of multilayer coating) or between the coating and the substrate usually limits the performance and life time of the coating [17]. Figure 7 depicts the result of the scratch test. Fig. 7a and 7b shows the scratch exhibited by the pristine and modified SS substrate. These Figs. Were used here as a reference. It can be observed that the pristine SS substrate exhibits large mean scratch width of 63.78 µm as shown in Fig. 7a. This is due to its high surface finish which make it vulnerable to scratches. After modification (Fig. 7b), the mean scratch width reduces to 40.46 µm as evident from Fig. 7b. The reduction the mean scratch width was due to the formation of rough Fe_3O_4 on the surface of the substrate which makes it resistant to scratch. After depositing Ti and AlN coating prior to annealing, the sample exhibits an increased mean scratch with of 43.69 µm as shown in Fig. 7c than the modified substrate under the same loading condition. This is because the grains of the Ti and AlN are loosely distributed over the surface of the substrate and they are susceptible to any form of scratch due to poor adhesion before annealing. However, after annealing the sample at 450 ^{o}C, the mean scratch width decreased drastically to 31.68 µm as shown in Fig. 7c. This is because the grains of Ti and AlN clings to one another and to the substrate, thus indicating good adhesion strength. Similar result was observed and reported elsewhere [12].

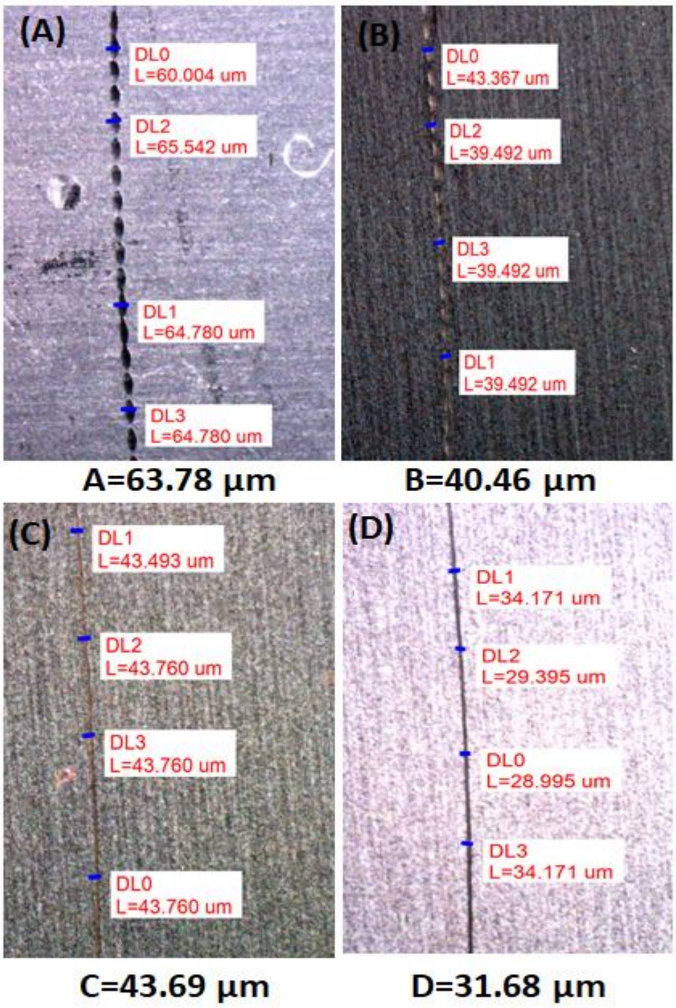

Fig. 7. Microscopic view of average scratch width of co-sputtered Ti and AlN under 1kgf load.

4. Conclusion

The study presents Ti and AlN composite coating deposited on to the modified SS substrate using DC/RF magnetron co-sputtering technique at room temperature towards improving the performance of concentrated solar thermal collectors for power generation. The coating exhibited high solar absorptance of 0.91 with god thermal stability of 45 ^{o}C in air. The high solar absorptance is attributed to the 'spongy' like structure and the surface roughness of the coating as revealed by the FESEM and AFM analysis respectively. Also, the intrinsic properties of the Fe_3O_4 plays a vital role in absorbing the incident solar radiation as evident from the UV-Vis analysis where the reflectance from the pristine substrate was supressed after the modification of the substrate due to the formation of Fe_3O_4. The adhesion strength of the coating is generally satisfying reduced mean scratch width after annealing. The high solar absorptance and good adhesion strength between the coating and the substrate even after annealing suggest its potential applicability towards improving the performance of the concentrated solar thermal collectors for power generation.

Acknowledgements

The authors thank the Tertiary Education Trust fund (TetFund) Nigeria for funding this research and the college management for approving the research.

References

[1] M. Bello and S. Shanmugan, "Achievements in mid and high-temperature selective absorber coatings by physical vapor deposition (PVD) for solar thermal Application-A review," *J. Alloys Compd.*, vol. 839, p. 155510, 2020, doi: 10.1016/j.jallcom.2020.155510.

[2] M. Bello and S. Shanmugan, "High-temperature AlN and Ti multilayer cermet for solar absorber coating : structural and optical properties," 2022, doi: 10.1007/s12648-022-02334-y.

[3] C. E. Kennedy, "Review of Mid- to High- Temperature Solar Selective Absorber Materials Review of Mid- to High- Temperature Solar Selective Absorber Materials," no. July, 2002.

[4] K. P. Ranjith, U. Basavaraju, H. C. Barshilia, and B. Basu, "Solar Energy Materials and Solar Cells On the origin of spectrally selective high solar absorptance of TiB 2 -based tandem absorber with double layer antireflection coatings," *Sol. Energy Mater. Sol. Cells*, vol. 220, no. June 2020, 2021.

[5] M. Bilokur, A. R. Gentle, M. D. Arnold, M. B. Cortie, and G. B. Smith, "High temperature optically stable spectrally-selective Ti1-xAlxN-based multilayer coating for concentrated solar thermal applications," *Sol. Energy Mater. Sol. Cells*, vol. 200, no. March, pp. 1–7, 2019, doi: 10.1016/j.solmat.2019.109964.

[6] L. Chaoying, S. Zhiqiang, H. Feng, Z. Hebin, and M. Juanrong, "Design, synthesis and thermal stability study on graded TiNxOy solar selective absorbing coating fabricated by pulsed DC reactive magnetron sputtering," *Mater. Charact.*, vol. 173, no. January, p. 110921, 2021, doi: 10.1016/j.matchar.2021.110921.

[7] T. C. Rojas, A. Caro, G. Lozano, and J. C. S, "Solar Energy Materials and Solar Cells High-temperature solar-selective coatings based on Cr (Al) N . Part 1 : Microstructure and optical properties of CrN y and Cr 1-x Al x N y films prepared by DC / HiPIMS," *Sol. Energy Mater. Sol. Cells J.*, vol. 223, no. December 2020, 2021.

[8] A. Dan, A. Biswas, P. Sarkar, S. Kashyap, and K. Chattopadhyay, "Solar Energy Materials and Solar Cells Enhancing spectrally selective response of W / WAlN / WAlON / Al 2 O 3 – Based nanostructured multilayer absorber coating through graded optical constants," *Sol. Energy Mater. Sol. Cells*, vol. 176, no. November 2017, pp. 157–166, 2018, doi: 10.1016/j.solmat.2017.11.013.

[9] H. X. Guo *et al.*, "Double-layer solar absorber coating based on high entropy ceramic AlCrMoTaTiN: Structure, optical properties and failure mechanism," *Surfaces and Interfaces*, vol. 24, no. November 2020, p. 101062, 2021, doi: 10.1016/j.surfin.2021.101062.

[10] X.-H. G. Y. Dong-Mei , Cheng-Yu He, Xiao-Li Qiu, Shuai-Sheng Zhao, Hui-Xia Guo, Gang Liu, "A multilayer solar absorber coating based on NbMoTaW refractory high entropy alloy: Optical properties, thermal stability and failure mechanism," *Mater. Today Energy*, 2021, doi: https://doi.org/10.1016/ j.mtener.2021.100789.

[11] J. Jyothi, S. Latha, P. Bera, H. S. Nagaraja, and H. C. Barshilia, "Optimization of process parameters to achieve spectrally selective TiAlC/TiAlCN/TiAlSiCN/TiAlSiCO/TiAlSiO high temperature solar absorber coating," *Sol. Energy*, vol. 139, pp. 58–67, 2016, doi: 10.1016/j.solener.2016.09.010.

[12] M. B and S. Shanmugan, "Investigation of in-plane heat distribution, thermal stability and mechanical properties of SS-(Fe3O4)/Ti/AlN/Ti/SiO2 as absorber coatings for efficient high temperature concentrated solar power systems," *J. Alloys Compd.*, vol. 901, p. 163576, 2022, doi: 10.1016/j.jallcom.2021.163576.

[13] C. Wang, J. Shi, Z. Geng, and X. Ling, "Polychromic Al-AlN cermet solar absorber

coating with high absorption efficiency and excellent durability," *Sol. Energy Mater. Sol. Cells*, vol. 144, pp. 14–22, 2016, doi: 10.1016/j.solmat.2015.07.049.

[14] M. Bello, S. Subramani, M. Marzaini, and B. Mohd, "Results in Physics The impact of Fe 3 O 4 on the performance of ultrathin Ti / AlN / Ti tandem coating on stainless-steel for solar selective absorber application," *Results Phys.*, vol. 19, no. November, p. 103582, 2020, doi: 10.1016/j.rinp.2020.103582.

[15] J. Feng *et al.*, "Solar selective absorbing coatings TiN/TiSiN/SiN prepared on stainless steel substrates," *Vacuum*, vol. 121, pp. 135–141, 2015, doi: 10.1016/j.vacuum.2015.08.013.

[16] E. Wäckelgård *et al.*, "Development of W-SiO2and Nb-TiO2 solar absorber coatings for combined heat and power systems at intermediate operation temperatures," *Sol. Energy Mater. Sol. Cells*, vol. 133, pp. 180–193, 2015, doi: 10.1016/j.solmat.2014.10.022.

[17] P. Ma, Q. Geng, X. Gao, S. Yang, and G. Liu, "Solution combustion of spinel CuMn2O4 ceramic pigments for thickness sensitive spectrally selective (TSSS) paint coatings," *Ceram. Int.*, vol. 42, no. 10, pp. 11966–11973, 2016, doi: 10.1016/j.ceramint.2016.04.122.